Fire Safety Journal 162 (2026) 104739

Contents lists available at ScienceDirect

Fire Safety Journal

journal homepage: www.elsevier.com/locate/firesaf

Burning of liquid pools and wood cribs in large fully developed timber compartment fires

Vinny Gupta [a,*], Keon Senez [a], Ian Pope [b], Felix Wiesner [c], Andrea Lucherini [d,1], David Lange [e,1], José L. Torero [f], Elizabeth Weckman [a,1], Juan P. Hidalgo [e]

[a] Department of Mechanical and Mechatronics Engineering, University of Waterloo, 200 University Ave., Canada
[b] The Danish Institute of Fire and Security Technology, Denmark
[c] Department of Wood Science, The University of British Columbia, Canada
[d] Department for Fire-Safe Sustainable Built Environment (FRISSBE), Slovenian National Building and Civil Engineering Institute (ZAG), Slovenia
[e] University of Queensland, St Lucia, QLD, 4072, Australia
[f] University College London, Gower St, London, United Kingdom

ARTICLE INFO

Keywords:
Compartment fires
Burning rates
Pool fires
Wood cribs
Protection of wood

ABSTRACT

The contribution of exposed mass timber to compartment fire dynamics is often framed by prescribed fuel load density, implicitly assuming fuel-independent thermal feedback. This paper interrogates that assumption experimentally using full-scale cross-laminated timber (CLT) compartments with two exposed surfaces (ceiling and side wall) and a movable fuel; either a kerosene pool or a wood crib. High-resolution measurements of heat flux, in-depth timber temperatures, burning rates, opening flows, and gas species demonstrate that fuel chemistry and geometry strongly modulate oxidizer delivery and residence time, thereby governing radiative feedback, CLT burning rates, and external flaming. The pool fire exhibited pronounced radiative enhancement and transient oxidizer starvation near the timber until pool decay. In contrast, the crib burning rate was inhibited, while the CLT burned efficiently. Analysis of the Global Equivalence Ratio (GER) and air bypass ratio revealed significant excess oxygen in the outflow, indicating that entrained air did not permeate the crib but instead oxidized the CLT, leaving unreacted air due to short mixing timescales. Despite unchoked doorway conditions, the crib fire produced bypass ratios and external flaming fractions comparable to the pool fire. The work shows that fuel load and ventilation factors alone are insufficient to describe the mass timber compartment fire dynamics and the CLT performance (e.g. charring). The fuel chemistry, geometry, and placement interact significantly with the compartment geometry. Therefore, the role of the moveable fuel is fundamental, and care must be employed when extrapolating demonstrator experiment results to the fire safety design of mass timber buildings.

1. Introduction

The contribution of exposed timber engineered products to the evolution of a compartment fire has received significant attention [1]. The interaction of the burning fuel load in a compartment fire and exposed timber is closely coupled, defining gas-phase conditions (i.e., temperatures, species concentrations, heat fluxes), flame spread, timber charring, and external flaming. These parameters have been the subject of study in numerous large-scale experiments featuring exposed timber, and a movable fuel (typically positioned on the floor) that is designed to achieve a target fuel load (typically in units of MJ/m^2_{floor}) based on prescribed fuel load densities.

Specification of fuel load provides a convenient metric for experimental design; however, it abstracts from the role of the fuel structure and chemistry, and its interaction with the compartment geometry and burning timber surfaces. Experiments have primarily relied on surrogate fuels such as wood cribs and/or furniture [2–8], with fuels arranged over a selected floor area to achieve the prescribed fuel loads. Such fuels, while useful for standardization, may not represent contemporary non-cellulosic fuels encountered in modern buildings, nor do they

This article is part of a special issue entitled: FISJ_IAFSS 2026 published in Fire Safety Journal.

* Corresponding author.
E-mail address: vinny.gupta@uwaterloo.ca (V. Gupta).

[1] The author [David Lange, Elizabeth Weckman, Andrea Lucherini, PhD] is an editor of this journal. In accordance with policy, [David Lange, Elizabeth Weckman, Andrea Lucherini, PhD] was blinded to the entire peer review process.

https://doi.org/10.1016/j.firesaf.2026.104739
Received 25 September 2025; Received in revised form 15 February 2026; Accepted 15 March 2026
Available online 20 March 2026

consider the coupling interaction of the exposed mass timber and the fuel itself [9]. Further, the selection of fuel, its fuel load and floor projected area are important parameters governing the fuel geometry. The assumption that a common fuel load produces comparable fire conditions between experiments neglects the importance of fuel geometry, chemistry, and compartment interactions and how those define the burning rates of the fuel and exposed timber.

It has been well-established in the compartment fire literature that for non-combustible compartment surfaces, wood crib fueled fully-developed compartment fires are relatively insensitive to elevated temperatures and thermal feedback, instead scaling with the ventilation factor, $A_o\sqrt{H_o}$ [10,11]. The ventilation factor controls the combustion efficiency of the cellulosic fuel [12]. By contrast, large mass transfer number (B-number) fuels such as plastics or liquid pools [13], are sensitive to radiative enhancement leading to accelerated burning rates relative to open burn conditions [14]. This creates a strong coupling between unburned fuel production and available oxygen. As fuels with large mass transfer numbers demand more oxygen per unit mass (about three times greater than cellulose), they can choke the compartment inflow, shifting burning to outside the compartment, thereby reducing interior thermal feedback [15,16]. At large-scales, hydrostatic conditions are generally not obtainable, and therefore strong inertial flows dominate the compartment interior [17], creating scalar gradients that can support localized burning and feedback [18]. For this reason, a high resolution of instrumentation is also required to characterize such localized phenomena.

Although timber compartment fires fueled by wood cribs and furnishings have been studied extensively, very few large-scale experiments have investigated the coupling between these fires and burning timber surfaces. This is an important gap that should be addressed as burning timber generates significant radiation [19,20], thus introducing the possibility for significant interaction with the fuel. The extent to which this coupling modifies fire development, ventilation dependence, and external flaming remains poorly understood.

This paper presents an analysis of large-scale compartment fire experiments with exposed cross-laminated timber (CLT) surfaces. Both a liquid pool fire and wood crib were employed as movable fuels. The fuels are designed to have the same nominal fuel load and effective burning diameter, providing a controlled basis for comparison. The wood crib represents a low mass transfer number fuel, relatively insensitive to external feedback, while the liquid pool represents a high mass transfer number fuel that is strongly affected by radiative enhancement with large air requirements. By analyzing the fuel and CLT burning rates, wall heat fluxes, inflow and outflow rates, and oxygen depletion, this study seeks to elucidate how fuel type interacts with burning CLT surfaces. In doing so, it highlights the limitations of fuel-load-based experimental approaches and provides new insight into the coupled role of fuel type, geometry, and area of exposed timber in governing compartment fire behavior.

2. Methodology

The experiments discussed herein (Tests 1.2, 2.2 and 4.1) form a focused subset of a larger full-scale mass-timber compartment testing campaign. Comprehensive details of the broader program, facility, and test methodology are reported in previous studies [21].

Experiments were conducted in full-scale compartments constructed from cross-laminated timber (CLT) panels. The internal dimensions of each compartment were 3.15 m × 3.15 m × 2.70 m, with a single front opening 0.85 m wide by 2.10 m high, corresponding to an inverse opening factor of 17.6 $m^{0.5}$. The CLT panels were 125 mm thick, manufactured from radiata pine in a three-layer layup of 45–35–45 mm, bonded with Purbond HBS polyurethane adhesive. The measured CLT density was 485 kg/m^3, with a moisture content of 10-14 %. To protect instrumentation located beneath the test space, a non-combustible false floor reduced the effective internal height from 3.00 m to 2.70 m.

The level of timber exposure was controlled by encapsulation. Two surfaces were left exposed in Test 2.2 and Test 4.1: the side wall 'D' and ceiling-panel 'E' (Fig. 1a). This corresponded to an exposed surface ratio, $A_{CLT}/A_T = 0.35$. All remaining surfaces were protected by two layers of 13 mm fire-rated gypsum plasterboard mechanically fastened with screws to the CLT substrate.

Two movable fuel configurations were employed. In Test 2.2, a kerosene pool fire was used, consisting of a square steel pan (1.0 m × 1.0 m plan area, 0.1 m depth) located at the compartment centre. Kerosene was supplied from an external tank through a controlled refilling system to ensure continual fuel supply, and a controllable shut-off [21]. Fuel supply was maintained for approximately 10 min following flashover, providing a post-flashover duration that allowed observation of timber involvement while avoiding premature failure of encapsulation layers. The net heat of combustion of kerosene under ideal conditions was assumed to be 44.1 MJ/kg, yielding a cumulative target fuel load of 318 MJ/m^2_{floor}. Test 1.2 is a reference test for Test 2.2, which features a pool fire with the same cumulative fuel load, but is fully-encapsulated such that $A_{CLT}/A_T = 0$ and will be used to benchmark the effects of CLT enhancement on the fuel burning rates.

Test 4.1 used a solid wood crib to replicate the fuel load energy, while altering the relationship of the compartment to the fuel. The crib was designed to match the estimated fuel load from Test 2.2 at 313 MJ/m^2_{floor} assuming a net heat of combustion of 17.5 MJ/kg. The total crib mass was 177.5 kg, cut from kiln-dried softwood into sticks of 1000 × 45 × 45 mm. Fourteen alternate layers were stacked orthogonally to form a structure 1000 × 1000 × 630 mm, with a uniform spacing of 45 mm, such that the crib porosity satisfies the open-regime [22]. The crib was ignited with four trays of 0.4 L kerosene each and was permitted to burn without external refueling. The exposed surface area of the crib, A_s was calculated to be 8 m^2 [23].

Thin-skin calorimeters (TSCs) were embedded flush with the exposed and encapsulated surfaces of the walls and ceiling (Fig. 1b). The TSCs, each constructed from a vermiculite body and a central Inconel disc are calibrated to infer the incident radiant heat flux from a heat balance [24]. In-depth thermocouples were embedded in the CLT panels from the rear at approximately the same location as the TSCs at eight depths (5, 10, 20, 30, 45, 60, 80, and 100 mm) from the exposed surface to track the progression of heating through the lamellae and across glue lines. Thermocouples were 1.5 mm in diameter, mineral-insulated metal--sheathed type K. The in-depth thermocouples are not corrected for a thermal disturbance error, however given that these measurements are used to extract a pyrolysis propagation rate rather than report absolute values, the effect of this on the results is expected to be minimal [25]. At the opening plane, the same type of thermocouples were paired with eight bi-directional velocity probes (BDPs) to measure gas inflow and outflow profiles (Fig. 1b) [26]. The bottom four probes were spaced at increments of 300 mm, with the top four spaced at 200 mm. Probe-transducer assemblies were calibrated for low Reynolds number flows [27], ensuring validity in both inflow and outflow regimes.

Oxygen, carbon dioxide, and carbon monoxide concentrations were monitored using aspirated gas analysers. Four sampling probes were located at two elevations near the opening: 0.675 m and 2.025 m. The probes were connected to a Non-Dispersive Infrared (NDIR) spectrometer analyser and an electrochemical O_2 analyser. The combination of these measurements enabled calculation of oxygen consumption calorimetry and provided an independent check against mass-loss calorimetry. The kerosene and wood crib were mounted on a 1 × 1 m load cell platform (300 ± 0.02 kg) to obtain real-time mass loss data. The external fuel supply rate for the kerosene pool re-filling system was measured using a calibrated ultrasonic flowmeter.

All tests were initiated using a small pilot flame. Flashover was defined as the point at which the upper-layer thermocouples recorded an average gas temperature of 600 °C. To facilitate comparison between fuels, the experimental timelines were normalized such that t =

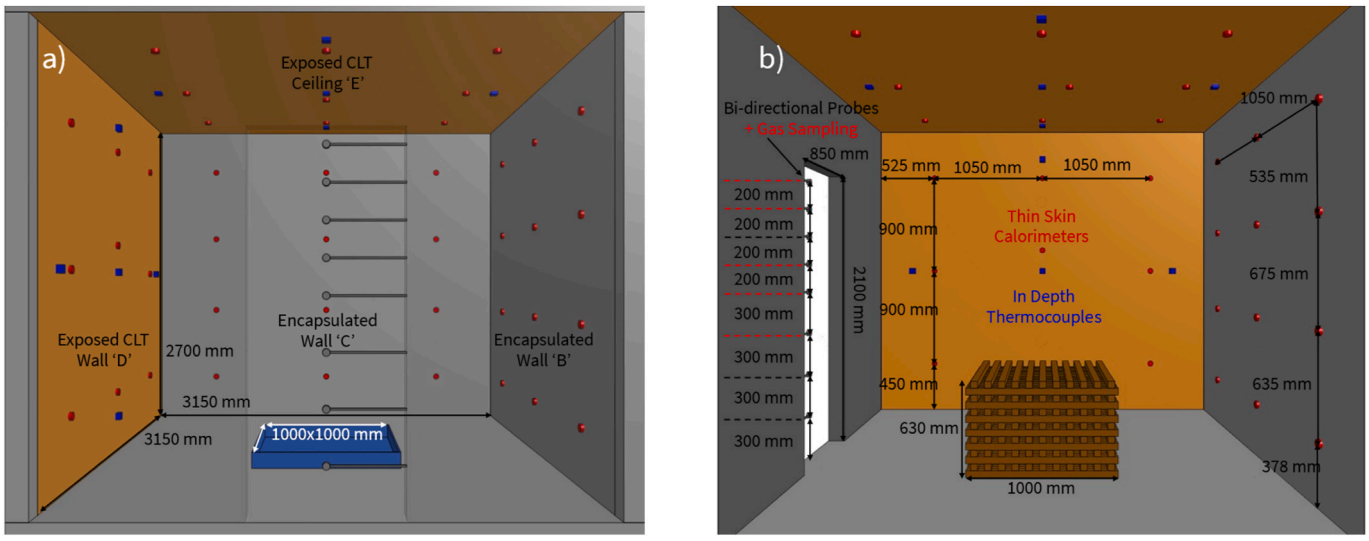

Fig. 1. Front (a) and side view (b) of the compartment geometry, fuel arrangement(s), and instrumentation layout relevant to this test.

0 corresponds to flashover. This offset for flashover was 60 s for the pool fire and 240 s for the wood crib fire. Data from all sensors were recorded at 1 Hz until either fuel burnout or test termination. More details on experimental setup available elsewhere [21].

3. Results

The condensed fuels studied in this experiment represent two limits of mass transfer numbers. The compartment geometry is designed to emulate ventilation-controlled conditions such that the fuel burning rate is dependent only on $A_0\sqrt{H_0}$, however the validity of this framework with the addition of exposed CLT will be assessed in the forthcoming sections.

3.1. Movable fuel burning rates

The instantaneous pool burning rate is quantified by applying a mass balance to the pool, which is treated as a control volume, such that $\dot{m}_b = \dot{m}_{f,flow} - dm/dt$ where $\dot{m}_{f,flow}$ is the inflow rate of kerosene from the balance tank and dm/dt is the pool mass loss rate (MLR) measured using a load cell placed underneath the pan. In Test 2.2, the fuel supply system was shut off at approximately 9 min after flashover, at which time the kerosene remaining in the tray and the line (from the tank) is allowed to be completely consumed. The wood crib burning rate in Test 4.1 is quantified by estimating the MLR of the crib on the load cell. For both tests, the noise in the load cell is first filtered using a Savitsky-Golay filter on the raw mass data. The MLR is calculated using a five-point central differencing scheme and is subsequently filtered using a moving average filter to reject noise.

The time-evolution burning rates for the pool fire and wood crib experiment are shown in Fig. 2a, along with the 95% confidence intervals of the noise distribution shown as a shaded region, and is defined from the raw pre-smoothed signal. For the pool fire, the liquid level continues to drop, and a steady burning rate is obtained until 5 min. The kerosene flow rate continues to increase, resulting in the total fuel burning rate rising to 0.11 kg/s at 9 min, at which time the fuel supply is cut, resulting in a decay in burning rate until total fuel consumption occurs at 20 min. The rise in burning rate at 5 min indicates a sudden change in the compartment thermal environment (noting that flashover has already been attained) resulting in increased thermal feedback.

The mean wood crib burning rate is larger than that of the pool fire. The shaded areas represent the 95% confidence intervals of the raw

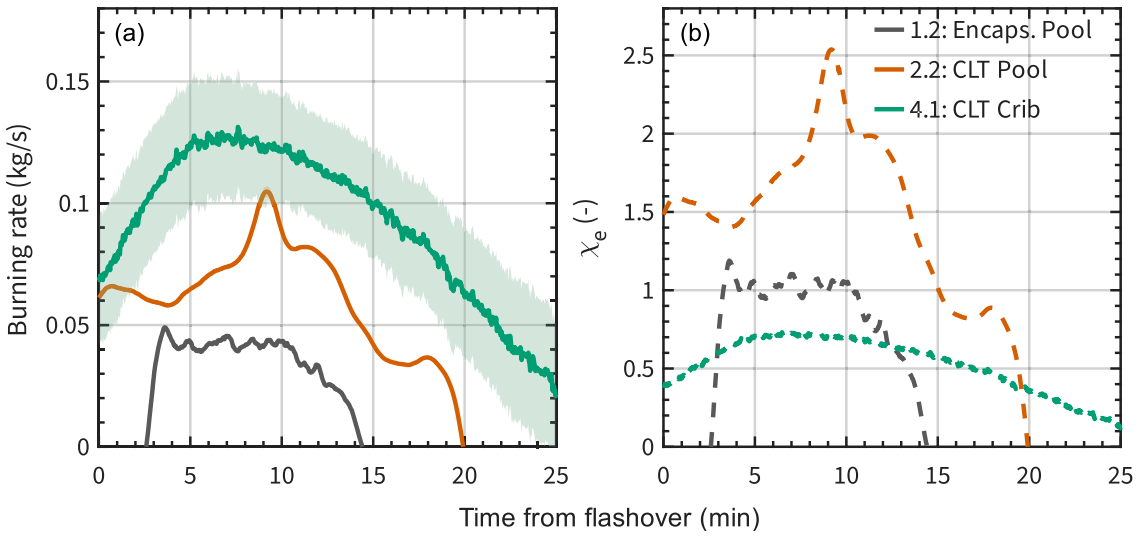

Fig. 2. (a) Time-evolution of the mass burning rate of the pool fire and wood crib, and (b) the burning rate enhancement factor.

signal, showing larger variation compared to the pool fire due to high measurement noise from the load cell and the thermomechanical effects of the crib sticks in aggregate (i.e., thermal expansion and cracking). Burning rates peak at approximately 0.13 kg/s, occurring at around 6 min after flashover, with a continual decay in burning rate until approximately 30 min. It should also be noted that burning continues past this point as char-fall off occurs, enabling re-ignition to occur, however, the data is truncated to 25 min to solely elucidate the fuel effects on the fully developed burning period.

Aside from the stoichiometric air-to-fuel requirements of kerosene and softwood, the selected fuels represent a dichotomy in compartment fire experiments as liquid hydrocarbon fuels are highly sensitive to external heat feedback effects due to significantly smaller heats of gasification [28] and the thermal properties of the liquids themselves, which facilitate in-depth heating through a range of modes, enhancing the burning rate [29]. Estimating thermal feedback effects on wood cribs is challenging as the porous structure of the crib shields the exposed inner vertical surfaces of the sticks, which burn in boundary layers in the open shafts, driving the total burning rate [18].

Given that the flaming CLT surfaces in the compartment increase both the temperature and heat flux fields [20], it is critical to assess the extent of radiative enhancement on the burning rate. To assess this, open burns of the pool fire and wood crib utilizing the exact same fuel loads as Tests 2.2 and Test 4.1 were undertaken to estimate the free burning rate, $\dot{m}_{p,free}$, by averaging the steady-state MLR. For the kerosene pool fire, $\dot{m}_{p,free\_pool} = 0.041$ kg/s and for the wood crib, $\dot{m}_{p,free\_crib} = 0.176$ kg/s. Therefore, a burning rate enhancement factor can be defined as

$$\chi_e = \dot{m}_{p,fuel} / \dot{m}_{p,free} \quad (1)$$

Fig. 2b shows the burning rate enhancement factor, χ_e on both the pool fire and wood crib. In Test 2.2, significant radiative enhancement on the kerosene pool burning rate is obtained from flashover, peaking at 2.5 prior to the fuel supply being shut. For reference, an inferred value for the burning rate for Test 1.2 (full encapsulation) is also shown on Fig. 2. Due to faulty mass loss measurements for this test, it was necessary to infer this value from the total heat release rate data [19] and by assuming the complete combustion of the kerosene. This is likely a slight overprediction of the burning rate, but it serves to highlight the effect of the exposed CLT on the burning rates in Test 2.2 and Test 4.1, where the burning rate is explicitly measured. The burning rate for Test 1.2 is lower than the corresponding pool fire test featuring two exposed CLT surfaces by between 20 and 100 %. The burning rate enhancement factor during the steady-state burning period approximates unity, therefore the radiative enhancement controlling the burning rate of the kerosene pool is exclusively due to the flaming CLT surfaces rather than the hot plasterboard.

Radiative enhancement factors are universally sub-unity for the wood crib in Test 4.1, varying between 0.4 and 0.7 during the fully-developed burning of the crib after flashover. The sub-unity values suggest that any radiative enhancement from the re-radiating CLT onto the outer-exposed surfaces of the crib are inhibited by an apparent reduction in oxidizer transport within the crib itself, thereby reducing the burning rate. Reductions in crib burning rate in compartments are extensively reported in the literature for conventional non-timber compartments [30]. However, combustion inhibition is closely related to the compartment reaching ventilation-controlled conditions, where choked conditions at the opening are obtained, resulting in reductions of the char oxidation within the crib itself, which is a key mechanism driving self-sustained burning [31]. Harmathy postulates zonal burning occurring inside the crib, where preferential burning and oxidation occurs at the side facing the compartment opening [15]. It is possible that the large crib geometry (1 × 1 m x 0.72 m) may induce significant flow resistances either in the horizontal or vertical shafts despite the large porosity [32]. Under these conditions, the crib may act as a bluff body, stalling entrained inflow air. Resulting recirculating air inside the compartment may be entrained by the CLT walls. Recent measurements of wood cribs in large compartment fires featuring shallow heights that are subject to intense external radiation from radiating flaming ceilings and walls by Hadden et al. [3] and Hidalgo et al. [33] show burning rate enhancements by up to two times. The fact that our results show the opposite finding of burning inhibition suggests that the crib geometry and its interaction in the compartment fire is highly relevant. It has been previously shown that flow velocities inside the compartment are large and thus mixing timescales are restricted by the characteristic residence time of the fire-induced flow [20]. It is important to note that no plume tilting was visible from the crib, unlike the pool fire test, thus the crib appears to behave almost like a bluff body obstructing the flow.

3.2. Spatial distribution of heat fluxes

Heat flux measurements from wall-mounted sensors were interpolated onto a uniform grid using cubic interpolation, and contours were plotted with a fixed color scale, as shown in Fig. 3. Heat flux measurements from wall-mounted sensors were interpolated onto a uniform grid using cubic interpolation, and contours were plotted with a fixed color scale. To reduce short-term variability, time-averaging was applied based on power spectral density analysis. Test 2.2 employed a 100 s averaging window, corresponding to compartment-scale oscillations of ~100 s, while Test 4.1 used a 50 s window, matching oscillations of ~50 s. These oscillations are governed by large-scale fluid motions in the compartment that appear to be fuel-specific and will require further investigations in future.

The heat flux contour plots obtained from Test 2.2 and Test 4.1 reveal spatial and temporal patterns, reflecting the influence of fuel type and the exposed mass timber surfaces. During the early fully-developed stage of the pool fire (5.0 – 6.7 min), the heat flux distributions were highly heterogeneous, with localized regions of elevated exposure on the side wall 'B' and the ceiling 'E'. These contours reflect the momentum-driven flow field characteristic of pool fire experiments, in which the plume is tilted by the strong inflow of air through the opening. At later times (13.3–15.0 min), after the pool fire began decaying, where the region of peak heat flux shifted to the exposed CLT surfaces (side wall 'D' and ceiling 'E') with much higher magnitudes. A notable feature is the lower ceiling-level heat fluxes during steady burning compared to the walls, which can be attributed to the insulating effect of the optically thick smoke layer.

By contrast, the wood crib experiment exhibited different heat flux distributions. In the early fully-developed stage (7.5 – 8.3 min), the contours were comparatively symmetrical, with radiant fluxes distributed more evenly across all the walls and ceiling. Later in the test (15.8 – 16.7 min), heat fluxes remained elevated throughout the compartment, decaying more gradually than in Test 2.2. Even after visible flaming subsided. The contribution of the room and smouldering crib sustains median heat fluxes above 100 kW/m^2. Prolonged exposure precluded self-extinction of the timber surfaces, and combustion persisted until suppressed manually. Unlike in Test 2.2, the ceiling remained more directly exposed to radiation, as lower soot yields and stronger thermal stratification limited the insulation provided by the smoke layer.

3.3. Exposed CLT burning rates

Once a stable char layer has formed over each measurement location on the CLT wall (up to five thermocouple clusters distributed per wall, shown on Fig. 1b), the total burning rate of the exposed CLT walls can be approximated. This is undertaken by measuring the time-evolution of a propagating 300 °C isotherm, with the exact location inferred by interpolating a high-order polynomial to the in-depth thermocouples. The 300 °C isotherm is approximated to represent the pyrolyzing front for *radiata pine*. The instantaneous pyrolysis front propagation velocity (charring rate) at each thermocouple cluster is estimated using a Savitzky—Golay differentiating filter. This locally fits low-order

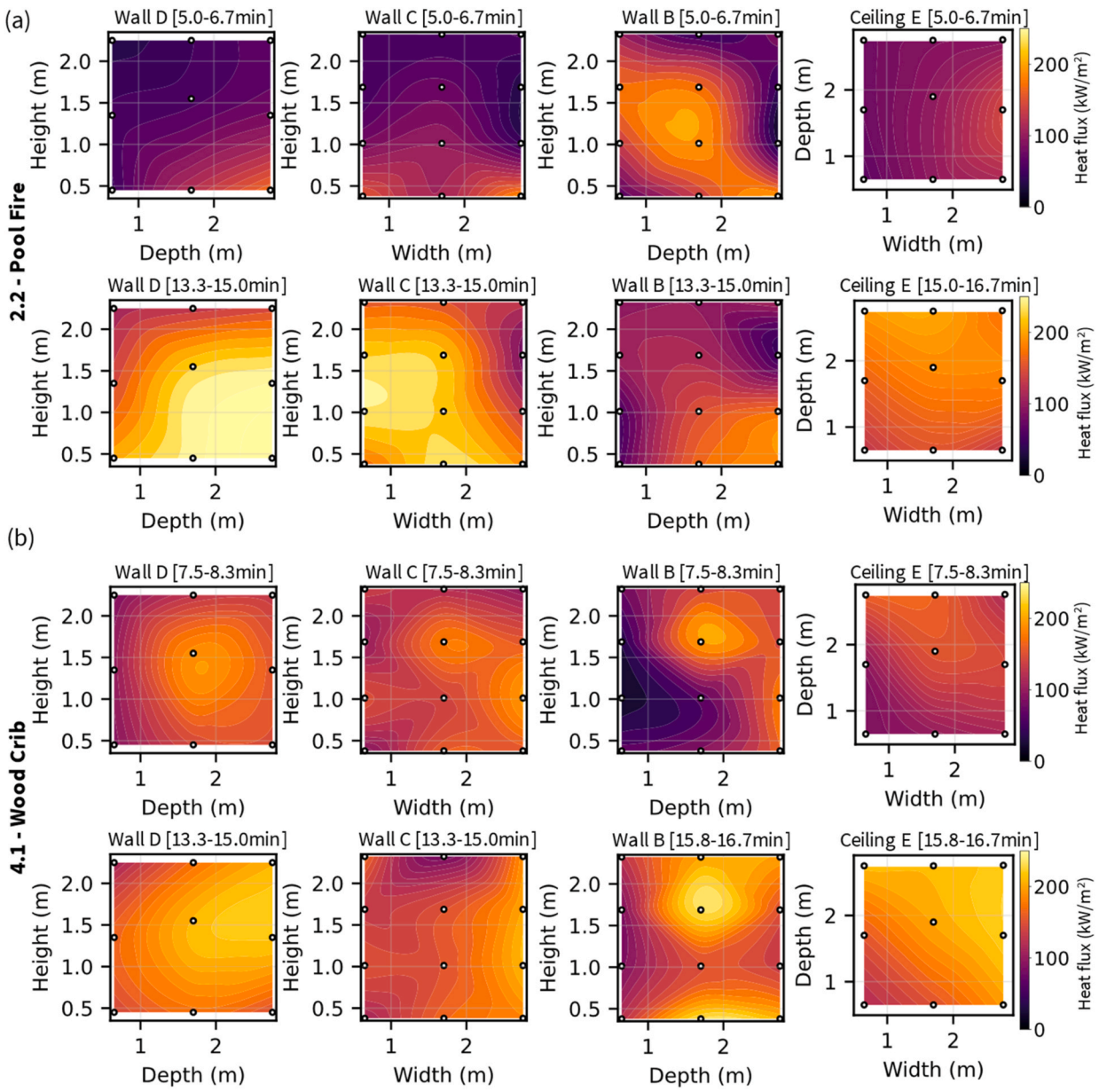

Fig. 3. Spatial contours of heat flux for CLT (side wall 'B', side wall 'D', and ceiling 'E') and non-CLT wall (back wall) for (a) Test 2.2 (pool fire), and (b) Test 4.1 (wood crib) during the fully-developed period.

polynomials to a moving window and evaluates their slope at the window center, suppressing noise to preserve an instantaneous readout of the burning rate [34]. The wall burning rates are calculated from

$$\dot{m}_{\mathrm{p,CLT}} = \rho_{\mathrm{CLT}} \eta \sum \dot{p}_i A_i \tag{2}$$

where $\dot{m}_{\mathrm{p,CLT}}$ is the burning rate of a given CLT wall or ceiling (kg/s), $\dot{p}_i$ is the local pyrolysis rate (m/s), A_i is the representative area of CLT for a thermocouple cluster over a wall (subscript i), ρ_{CLT} is the density of CLT (450 kg/m^3), and η represents the fraction of CLT that participates in pyrolysis, which is approximated as $\eta = 0.6$ from thermogravimetric data for *radiata pine* [33].

Fig. 4 shows the time-evolution of the spatially integrated burning rates for both the CLT ceiling and walls for both the pool fire and wood crib experiments. The movable fuel burning rate is superimposed for reference. In both experiments, steady-state charring occurs at 5 min, and thus the initial burning of the CLT is not reported. Peak wall burning rates in the pool fire test (Fig. 4a) are consistent for both CLT surfaces at 0.08 kg/s occurring at approximately 14 min. Peak wall burning rates lag the termination of fuel supply to the kerosene pool by 5 min, which is in the process of decaying at this point. Peak wall burning rates also coincide with the rise of heat fluxes on the CLT surfaces, suggesting that prior to the decay of the pool fire, there is insufficient air available to react with the pyrolyzing CLT surfaces. Additionally, the ceiling reaches steady state burning first, likely due to the formation of an optically thick smoke layer on the ceiling, which provides significant heating. The delay in the pyrolysis of the side wall may be linked to the local availability of oxygen and flow dynamics in the compartment. This is demonstrated by the fact that burning is observed (Fig. 3) on the opposite non-combustible surface (side wall 'B'), close to the floor during the fully developed portion of the kerosene fire. It is only when the fuel supply is cut that this trend shifts and preferential burning occurs over the CLT walls.

Fig. 4b shows the wall and ceiling CLT burning rates for the wood crib experiments, which peak at approximately 0.07 kg/s. Despite similar peak burning rates to the pool fire, no temporal lag with the peak

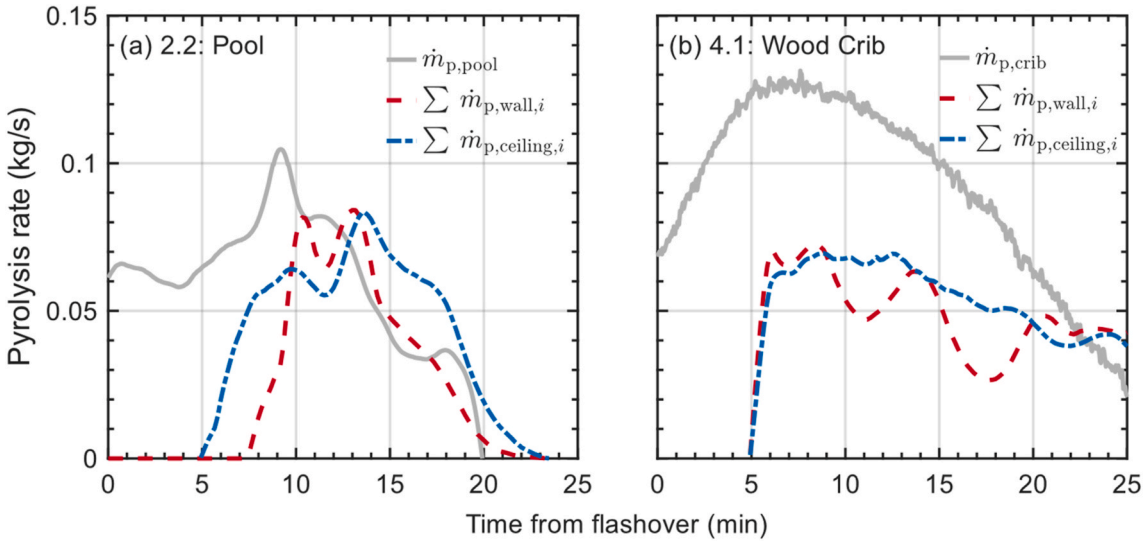

Fig. 4. Time-evolution of burning rates of CLT wall (red) and ceiling (blue) with movable fuel (gray). (For interpretation of the references to color in this figure legend, the reader is referred to the Web version of this article.)

crib burning rate occurs. Peak wall burning rates coincide with peak crib burning. Moreover, the magnitude and trend of both the ceiling and wall burning rates are very close, mirroring the homogeneous spatial distribution of heat fluxes identified earlier for the wood crib experiment. The lack of a delay and consistency of both the side wall and ceiling burning rates indicates that there is sufficient air to homogenously react with the pyrolyzing CLT surfaces. This reinforces the notion that the compartment is not choked in this case, and that the reduction in the crib burning rate is an artefact of the flow interaction with the crib geometry.

3.4. Compartment mass balance

The preceding analysis suggests that the flow conditions and oxygen transport to both the fuel and CLT surfaces are sensitive to the dynamics induced by the movable fuel load. To elucidate the fuel effect on the inflow and outflow rates, such that a determination on whether the flow at the doorway chokes, a time-resolved mass balance is performed on the compartment as a control volume, following Eq. (3).

$$\dot{m}_{out} = \dot{m}_{in} + \dot{m}_{p,fuel} + \sum \dot{m}_{p,CLT} \tag{3}$$

where $\dot{m}_{in}$ and $\dot{m}_{out}$ are the mass flow rates both in and out of the compartment, respectively. The doorway mass flow rates are calculated by the numerical integration of Eq. (4) and Eq. (5).

$$\dot{m}_{in} = C_d\, \rho_\infty w_o \int_0^{H_N(t)} v_{in}\, dz \tag{4}$$

$$\dot{m}_{out} = C_d w_o \int_{H_N(t)}^{H_T} v_{out} \rho_g\, dz \tag{5}$$

where v is the velocity, measured with bi-directional probes positioned at the centreline of the doorway, and ρ_g is the corresponding gas density is estimated based on the gas temperature measured using a local thermocouple close to each probe. Thermocouples positioned at the opening below the neutral plane in the inflow were impacted by radiation error, to correct for this the values were set to the ambient temperature [35]. The error in the outflow thermocouples is minimal and was not corrected [36]. C_d is the discharge coefficient at the doorway, that is assumed as 0.7 [37], though it should be noted that this varies over the height of the compartment [30], and is difficult in this case to estimate as hydrostatic conditions are not obtained [20]. H_N is the neutral plane height that is obtained by linear interpolation of the vertical flow profile, which is relatively constant during the fully developed period. The flow from the top and bottom probes are extended to $z = 0$ and $z = H_T$ assuming a top-hat distribution. Eq. (4) and Eq. (5) assume that the flow across the width, w_o, is uniform.

Fig. 5 shows the compartment mass balance for the: (a) pool fire and (b) wood crib experiments, with the inflow and outflow rates highlighted, along with the total mass contribution from the pyrolyzing movable fuel and CLT. The sum of the pyrolyzing fuel contributions is given by $\dot{m}_{p,tot}$, and when combined with the inflow mass flow rate, $\dot{m}_{in}$, represents the net input of mass into the compartment. The results show that conservation of mass (summation of the burning rate and mass inflow terms) is generally obtained to approximately 10 – 15 % of the outflow. This is particularly the case once fully developed burning conditions are obtained, where the contribution of the movable fuel and CLT production rates contributes substantially to the mass balance.

Fluctuations in the mass inflow rates are larger than the outflow rates and correlate with measured fluctuations in the burning rate, suggesting hysteresis effects in the flow profile. The mass inflow rates for the pool fire (Fig. 5a) increases between 1.0 and 1.1 kg/s as the pool fire burning rate and CLT contribution increases but then stagnates from 10 to 15 min. As the CLT burning rates decay at 15 min, inflow air rate increases which suggests that the doorway flow is choked during periods when the pool and CLT are burning. By comparison, the wood crib (Fig. 5b) has larger inflow rates between 1.3 and 1.6 kg/s during fully-developed burning. Kerosene has a stoichiometric air requirement that is three times greater than the wood used in the crib and yet the fuel burning rates for both fuels are similar. Therefore, the net air requirements for the pool fire are greater than the wood crib, and it is likely that choked flow conditions at the doorway occur for the pool. The validity of this approximation requires assessing oxygen depletion and the air requirements to deliver the burning rates obtained from the movable fuel and CLT, which is discussed in the proceeding section.

4. Internal burning mechanism

The framework developed by Kawagoe and Thomas for fully developed compartment fires presumes complete oxygen depletion in the compartment to enable choked inflow conditions [16]. Under these conditions, the theoretical air inflow rate is approximated as $\dot{m}_{in,th} = 0.52 A_o \sqrt{H_o}$, which corresponds to approximately 0.86 kg/s, and is a fuel-independent quantity [38]. The theoretical limit corresponds to the pre-shutoff period of the pool fire, indicating that the compartment

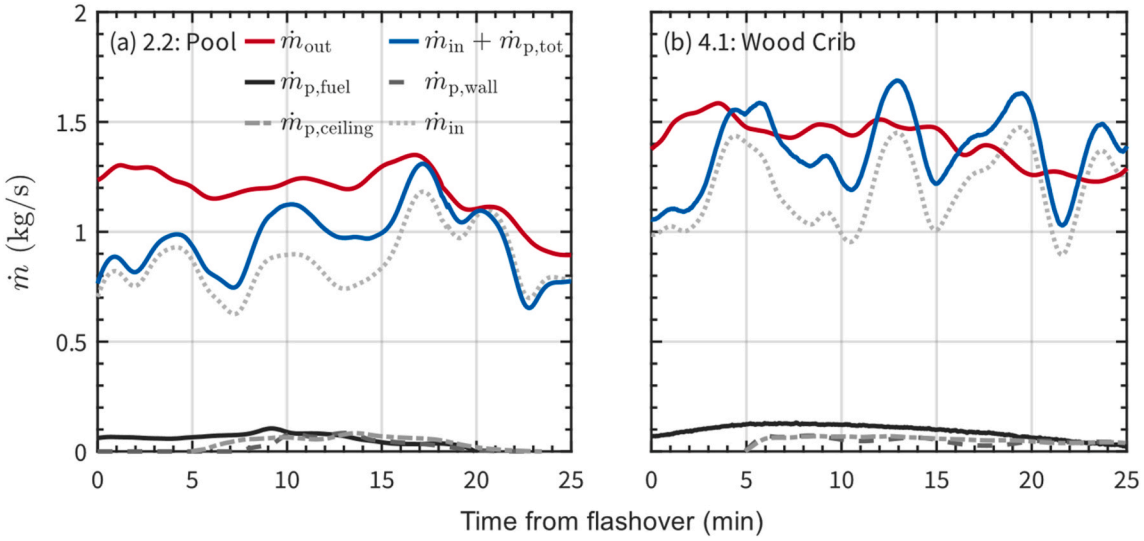

Fig. 5. Time-evolution of the reconstructed mass balance including the outflow flow rate, movable fuel mass loss rates, and CLT mass flow rates. (a) Test 2.2, (b) Test 4.1.

doorway is close to choked. However, during the post-shutoff period and for the wood crib test, both inflow rates are above the theoretical limit, highlighting that choked conditions are not obtained and that the extreme burning rate enhancement effects on the pool fire and excess fuel supply by the CLT may influence the limiting flow conditions. It is therefore necessary to evaluate the oxygen requirements for burning rates measured from the movable fuel load and exposed CLT to determine the nature of these discrepancies.

Oxygen depletion and combustion efficiency are assessed using the internal and doorway gas sampling probes, summarized in Table 1. Spatially averaged outflow and internal O_2 concentrations and CO/CO_2 ratios are reported for the pre- and post-fuel supply shut-off periods in the pool fire test, and over the fully developed burning region of the wood crib test. Prior to the shutoff of the kerosene supply in Test 2.2, O_2 concentrations in the outflow are at 1.4 %, which reduces to 0.62 % as the pool fire decays and the burning rate of the exposed CLT surfaces increases. This suggests that the cumulative oxygen requirements of the decaying pool fire and exposed CLT surfaces exceed the pool itself, and that transport of the O_2 into the walls is facilitated by the lack of available flame surface area associated with the burning pool. A notable observation is that with the wood crib, the O_2 concentration in the outflow is significantly larger than the pool fire at 6.4 %. This concentration was confirmed with a repeat experiment (unreported Test 4.2). There is considerable O_2 left unreacted in the compartment that is advected through the opening and confirms that the burning rate of the crib is inhibited by the inability of O_2 to permeate into the crib structure, rather than under-ventilated conditions being attained as found by Quintiere and McCaffrey [30]. Excess O_2 in the outflow suggests that the residence time in the compartment is too short, preventing mixing of the fuel and oxidizer inside the compartment.

Table 1
Spatially and temporally averaged O_2 mole fractions and CO/CO_2 ratios of the gas analysis probes at the doorway and inside the compartment.

	$X_{O_2,outflow}$ (%)	$[CO/CO_2]_{outflow}$ (−)	$X_{O_2,internal}$ (%)	$[CO/CO_2]_{internal}$ (−)
Test 2.2: Pool fire Pre-shutoff [2 – 8 min]	1.39	0.43	1.67	0.42
Test 2.2: Pool fire Post-shutoff [10 – 15 min]	0.62	0.52	1.69	0.71
Test 4.1: Wood crib [10 – 15 min]	6.40	0.29	5.67	0.33

To elucidate the burning mechanism for pool fires and wood cribs in the presence of exposed CLT, it is necessary to quantify the oxidizer requirements for the mass burning rates and develop a methodology by which the extent of mixing with fuel produced may be inferred. The ratio of the oxidizer requirements in the compartment to the oxygen exchange at the doorway is known as the global equivalence ratio (GER) [12], defined in Eq. (6). GER > 1 indicates excess fuel relative to available oxidizer at the compartment scale.

$$\mathrm{GER} = \frac{\sum \dot{m}_{p,i} r_{eff,i}}{Y_{O_2,in}\dot{m}_{in} - Y_{O_2,out}\dot{m}_{out}} \tag{6}$$

where the term $\sum \dot{m}_{p,i} r_{eff,i}$ is the sum of the product of the burning rate and the effective oxygen-to-fuel ratio of the movable fuel and CLT. The stoichiometric oxygen requirement per unit fuel was corrected for incomplete oxidation using the measured CO/CO_2 ratio, with carbon forming CO consuming 0.5 moles of O_2 and carbon forming CO_2 consuming 1 mole of O_2, yielding an effective requirement $r_{eff,i}$ as the weighted sum of the two pathways. Thus, for kerosene ($C_{12}H_{26}$), $r_{eff,C_{12}H_{26}} = 4.6\ kg_{air}/kg_{fuel}$ and *radiata pine* (48% C, 6% H, 46% O), $r_{eff,pine} = 13.5\ kg_{air}/kg_{fuel}$. $Y_{O_2,in}$ and $Y_{O_2,out}$ are the oxygen mass fractions determined from Table 1.

The fraction of oxygen leaving the compartment unreacted is defined in Eq. (7) as an air bypass ratio, which measures how effectively the available oxygen entering the compartment mixes with excess fuel once GER >1 and burns inside the compartment.

$$f_{bypass} = \frac{Y_{O_2,out}\dot{m}_{out}}{Y_{O_2,in}\dot{m}_{in}} \tag{7}$$

The time-evolution of the GER (left axis) and f_{bypass} (right axis) is shown in Fig. 6 for the (a) pool fire, and (b) wood crib experiments. The data confirms that prior to the involvement of exposed CLT, the GER varies between 1 and 1.2, and thus the compartment is consuming all the available air that is not bypassed. The GER doubles as the pool and CLT burning rate both increase past 6 min, demonstrating significant excess fuel production. f_{bypass} in this period is 10%, which implies that there is insufficient mixing to oxidize the abundant fuel inside the compartment. Based on the prior heat flux and wall burning rate data, it is now apparent that the flow induced by the pool fire plume inhibits the oxidizer from either reaching the exposed CLT surfaces or mixing with

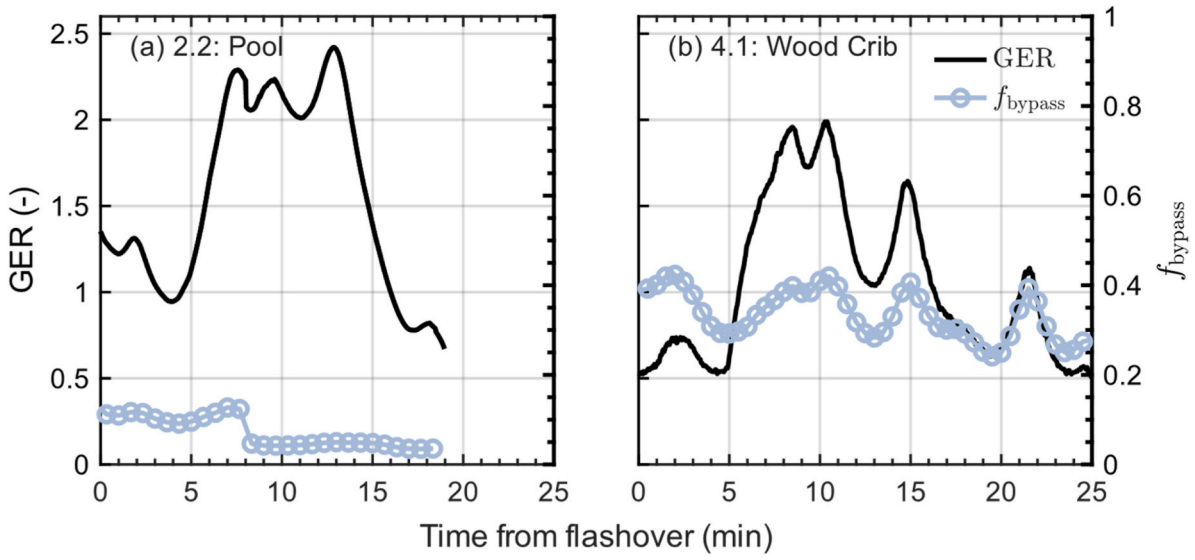

Fig. 6. Time-evolution of the GER (left axis), air bypass ratio (right axis), and internal heat release rate fraction (right axis), for (a) the pool fire, and (b) the wood crib experiments.

excess fuel, thereby reducing the overall combustion efficiency inside the compartment. Once the kerosene supply is shut at 9 min, the GER increases to 2.5 and the bypass ratio drops to 5% as oxidizer can now reach the CLT surfaces, increasing the fuel supply rate, and counteracting the decaying pool fire burning rate.

The GER for the wood crib in Fig. 6b increases to approximately 2 once both the crib and exposed CLT surfaces reach their peak burning rates. However, in this case, the GER is amplified by significant air bypass, which oscillates between 25 and 40%, and drives the poor combustion efficiency of the wood crib as the air cannot permeate through the crib and instead oxidizes the CLT surfaces. This phenomenon is an artefact of the crib geometry, rather than the attainment of ventilation-controlled conditions, despite the GER being consistent with the pool fire test. The comparatively large bypass to the pool fire experiment also demonstrates that the oxidizer residence timescales are too short to allow adequate mixing, likely due to turbulent flows generated by the reacting CLT surfaces, and possible local flow interaction resulting from the crib geometry.

Choked flow conditions are obtained for the pool fire, but not the wood crib. However, in both cases the bypass ratio shows that the compartment does not satisfy well-stirred conditions. Instead, the interaction of the movable fuel, CLT and compartment creates conditions where the burning is controlled by the interior flow conditions which determine the local distribution of oxidizer. Therefore, the flow cannot be governed by $A_o\sqrt{H_o}$. Instead, it is shown that the internal fire dynamics are highly sensitive to both the fuel type, but also the fuel geometry.

The combination of air bypass and excess fuel generation inside the compartment raises an open question into external flaming as more fuel is allowed to leave the compartment due to poor mixing, which cannot be quantified by $A_o\sqrt{H_o}$. The fraction of internal burning is:

$$\chi_{int} = \frac{E_{O_2}\left(Y_{O_2,in}\dot{m}_{in} - Y_{O_2,out}\dot{m}_{out}\right)}{\dot{Q}_{tot}} \tag{8}$$

where $E_{O_2} = 13100\ \mathrm{kJ/kg_{O_2}}$ [39], and $\dot{Q}_{tot}$ is the total heat release rate extracted from Wiesner et al. [19].

The internal burning fraction is shown in Fig. 7. Very similar fractions for both fuels are observed, varying between 40 and 60 % during the fully developed stage of the compartment fire. This similarity is despite the heating value for kerosene being almost 2 – 3 times greater than the wood crib and with the attainment of almost complete

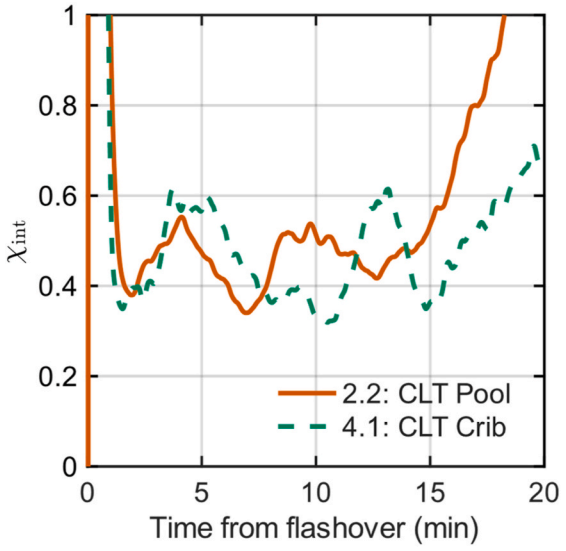

Fig. 7. Fraction of the internal heat release rate for Test 2.2 (pool fire) and Test 4.1 (wood crib).

consumption of the oxygen. Thus, for the wood crib test to maintain similar levels of internal burning in non-vitiated conditions, it indicates that the fluid mechanics governing the air bypass strongly influence the fractions of internal and external flaming for these fuels. This finding has significant implications for the assessment of external flaming in mass timber compartments featuring similar cellulosic-based fuel packages.

The burning conditions of the exposed CLT surfaces for both fuel sources can now be defined by transforming the coordinate system into GER space, as shown in Fig. 8. The color bar is normalized to 20 min from flashover, enabling a transformation of GER into a temporal space. The burning conditions of the exposed CLT surfaces show only a weak correlation with GER. Burning rates on Wall D are limited in the pool fire test, while the ceiling had peak burning rates across a range in GER. Comparatively in the crib test, similar peak CLT burning rates were observed across GER values between 1 and 2 on both the ceiling and the wall. These results are supported by reduced-scale studies [40].

The dispersion in peak burning rates highlights that GER struggles to capture the complexity of the timber burning. Instead, the results further

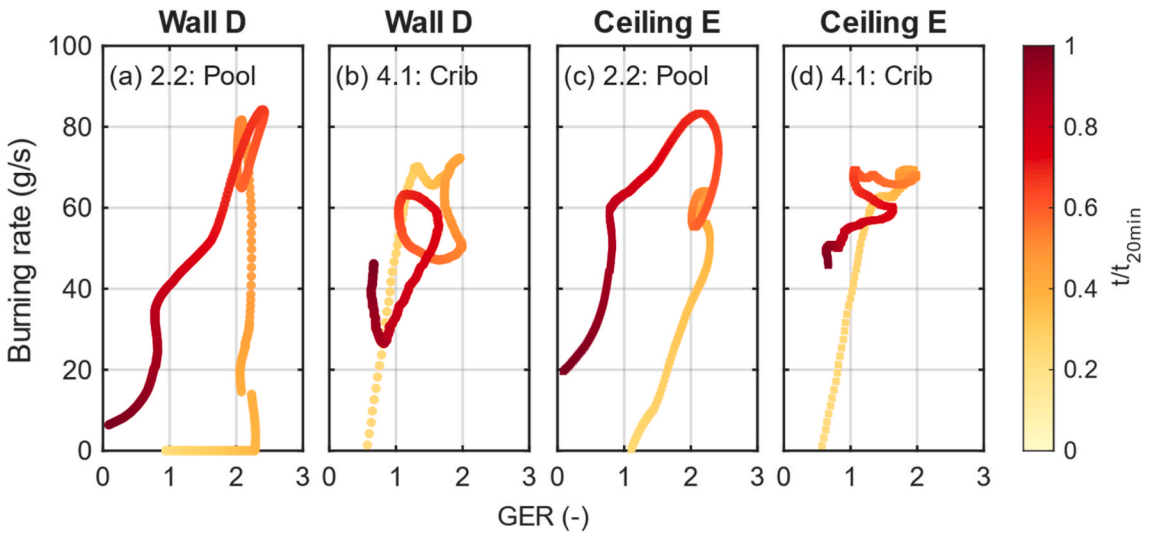

Fig. 8. Dependence of CLT burning rates on GER for the liquid pool and wood crib tests.

support that the spatial distribution of the oxidizer reaching the CLT surfaces drives the burning rates as discussed in preceding sections, and that increased oxidizer availability at the CLT walls throughout the duration of the crib test contributed to the span of GER with peak burning rates. Furthermore, these findings show that there is a great need for detailed, local measurements of oxygen availability near exposed timber surfaces.

5. Conclusions

This study demonstrates that prescribed fuel-load density alone is insufficient to characterize mass-timber compartment fires. Full-scale experiments with kerosene pool fires and wood cribs in cross-laminated timber compartments reveal that fuel type and geometry strongly influence internal flows, oxidizer distribution, and burning behavior.

The burning rate of the kerosene is strongly enhanced by the burning timber, choking the inflow of air into the compartment and limiting oxygen access to the timber surfaces. Once the pool fire starts to decay, the burning rates of the timber walls increase. In contrast, the wood crib burning rate is inhibited, however choked inflow conditions are not obtained, and the exposed timber surfaces burn more efficiently.

The global equivalence ratio (GER) and air bypass ratio are quantified to provide interpretation into the mixing efficiency and oxygen transport. In the pool fire, the GER is elevated by excess fuel production from kerosene and CLT, with 40 – 60 % of the total heat released externally. Air bypass ratios of ~10 % indicate that plume-driven inertial flows restrict mixing, and prevent full utilization of the available oxygen, which improves once the pool fire decays. For the wood crib, bypass ratios increase to 25 – 40 %, confirming that the compartment is not ventilation-controlled. Instead, the burning rate reduction of the crib occurs due to the inability for air to permeate through the crib structure. Short residence times in the compartment inhibit mixing, and therefore complete oxygen consumption. Despite threefold lower oxygen demand for wood compared to kerosene, both fuels produce comparable GER values and external flaming fractions. However, for wood cribs, this is an artefact of the air bypass that occurs in the compartment.

These results demonstrate that the well-stirred assumption underlying the compartment fire framework is not valid for mass-timber compartments. The fuel load and ventilation factor alone are insufficient to describe the compartment fire dynamics, and therefore the fire performance of exposed CLT (e.g. charring) is strongly influenced by the fuel chemistry, geometry, and placement relative to the opening. These fuel parameters control the local flow and oxidizer conditions inside the compartment. Therefore, the interpretation and extrapolation of large-scale test data for code development or design must be done with great caution due to the significant sensitivity of the CLT to the fuel type in a compartment fire.

CRediT authorship contribution statement

Vinny Gupta: Writing – original draft, Resources, Project administration, Methodology, Investigation, Formal analysis, Conceptualization. **Keon Senez:** Writing – original draft, Visualization, Formal analysis. **Ian Pope:** Writing – review & editing, Investigation, Formal analysis. **Felix Wiesner:** Writing – review & editing, Formal analysis. **Andrea Lucherini:** Writing – review & editing, Investigation. **David Lange:** Writing – review & editing, Supervision. **José L. Torero:** Writing – original draft, Investigation, Funding acquisition, Conceptualization. **Elizabeth Weckman:** Writing – original draft, Investigation. **Juan P. Hidalgo:** Writing – review & editing, Project administration, Methodology, Investigation, Funding acquisition, Conceptualization.

Declaration of competing interest

The authors declare that they have no known competing financial interests or personal relationships that could have appeared to influence the work reported in this paper.

Acknowledgements

This project was funded by the ARC Future Timber Hub (IH150100030) and received generous support from QFES, XLam, Hyne Timber, Lend Lease, Knauf and Rockwool International A/S. The authors are extremely grateful to QFES for providing their research facility and engagement with the project. Dr. Gupta and Dr. Weckman are supported by the NSERC Alliance program (Next Generation Wood Construction). Mr. Senez is supported by the NSERC CGS-M scholarship. Dr. Pope was supported by the Innovation Fund Denmark, the Danish Agency for Higher Education and Science, and DBI. Dr. Wiesner is supported by NSERC grant RGPIN-2024-04433. Dr. Lucherini would also like to gratefully acknowledge the financial support for the FRISSBE project within the European Union's Horizon 2020 research and innovation programme (GA 952395).

References

[1] A.A. Ali Awadallah, R.M. Hadden, A. Law, Meta-analysis of temperature, heat release rate, delamination and auto-extinction of timber compartments, Fire Saf. J. 146 (2024) 104164, https://doi.org/10.1016/j.firesaf.2024.104164.

[2] R. Emberley, C.G. Putynska, A. Bolanos, A. Lucherini, A. Solarte, D. Soriguer, M. G. Gonzalez, K. Humphreys, J.P. Hidalgo, C. Maluk, A. Law, J.L. Torero, Description of small and large-scale cross laminated timber fire tests, Fire Saf. J. 91 (2017), https://doi.org/10.1016/j.firesaf.2017.03.024.

[3] R.M. Hadden, A.I. Bartlett, J.P. Hidalgo, S. Santamaria, F. Wiesner, L.A. Bisby, S. Deeny, B. Lane, Effects of exposed cross laminated timber on compartment fire dynamics, Fire Saf. J. 91 (2017) 480–489, https://doi.org/10.1016/j.firesaf.2017.03.074.

[4] P. Kotsovinos, E. Rackauskaite, E. Christensen, A. Glew, E. O'Loughlin, H. Mitchell, R. Amin, F. Robert, M. Heidari, D. Barber, G. Rein, J. Schulz, Fire dynamics inside a large and open-plan compartment with exposed timber ceiling and columns: codered #01, Fire Mater. 47 (2023) 542–568, https://doi.org/10.1002/fam.3049.

[5] J. Su, P. Leroux, P.-S. Lafrance, R. Berzins, K. Gratton, E. Gibbs, M. Weinfurter, Fire Testing of Rooms with Exposed Wood Surfaces in Encapsulated Mass Timber Construction, 2018.

[6] H.R. Medina Hevia, Fire Resistance of Partially Protected Cross-Laminated Timber Rooms, Carleton University, 2014.

[7] J. Sjöström, D. Brandon, A. Temple, J. Anderson, R. McNamee, External fire plumes from mass timber compartment fires—Comparison to test methods for regulatory compliance of façades, Fire Mater. 47 (2023) 433–444, https://doi.org/10.1002/FAM.3129.

[8] L. Jiang, D. Zeinali, A. Steen-Hansen, M. Bergius, T. Li, Fire testing as a tool in fire safety engineering: a Norwegian perspective, Fire Mater. 0 (2025) 1–15, https://doi.org/10.1002/FAM.70006.

[9] T.Z. Harmathy, Postflashover fires - an overview of the research at the national research council of Canada (NRCC), 1970-1985, Fire Technol. 22 (1986) 210–233, https://doi.org/10.1007/BF01043125.

[10] K. Kawagoe, Fire Behaviour in Rooms, 1958.

[11] P.H. Thomas, A.J.M. Heselden, Fully Developed Fires in Single Compartments, 1972.

[12] A. Tewarson, Fully developed enclosure fires of wood cribs, Symposium (International) Combust. 20 (1985) 1555–1566, https://doi.org/10.1016/S0082-0784(85)80650-0.

[13] J.L. Torero, T. Vietoris, G. Legros, P. Joulain, Estimation of a total mass transfer number from the standoff distance of a spreading flame, Combust. Sci. Technol. 174 (2002) 187–203, https://doi.org/10.1080/713712953.

[14] M.L. Bullen, P.H. Thomas, Compartment fires with non-cellulosic fuels, Symposium (International) Combust. 17 (1979) 1139–1148, https://doi.org/10.1016/S0082-0784(79)80108-3.

[15] T.Z. Harmathy, Mechanism of burning of fully-developed compartment fires, Combust. Flame 31 (1978) 265–273, https://doi.org/10.1016/0010-2180(78)90139-6.

[16] P.H. Thomas, M.L. Bullen, Burning of fuels in fully-developed room fires, Fire Saf. J. 2 (1980) 275–281, https://doi.org/10.1016/0379-7112(79)90027-4.

[17] J.L. Torero, A.H. Majdalani, A.E. Cecilia, A. Cowlard, C. Abecassis-Empis, A. Cowlard, A.E. Cecilia, A. Cowlard, Revisiting the compartment fire, Fire Saf. Sci. 11 (2014) 28–45, https://doi.org/10.3801/IAFSS.FSS.11-28.

[18] V. Gupta, J.L. Torero, J.P. Hidalgo, Burning dynamics and in-depth flame spread of wood cribs in large compartment fires, Combust. Flame 228 (2021) 42–56, https://doi.org/10.1016/j.combustflame.2021.01.031.

[19] F. Wiesner, H. Xu, D. Lange, V. Gupta, I. Pope, J.L. Torero, J.P. Hidalgo, Large-scale compartment fires to develop a self-extinction design framework for mass timber-Part 2: results, analysis and design implications, Fire Saf. J. 152 (2025) 104346, https://doi.org/10.1016/j.firesaf.2020.103098.

[20] I. Pope, V. Gupta, H. Xu, F. Wiesner, D. Lange, J.L. Torero, J.P. Hidalgo, Fully-developed compartment fire dynamics in large-scale mass timber compartments, Fire Saf. J. 141 (2023), https://doi.org/10.1016/j.firesaf.2023.104022.

[21] H. Xu, I. Pope, V. Gupta, J. Cadena, J. Carrascal, D. Lange, M.S. McLaggan, J. Mendez, A. Osorio, A. Solarte, D. Soriguer, J.L. Torero, F. Wiesner, A. Zaben, J. P. Hidalgo, Large-scale compartment fires to develop a self-extinction design framework for mass timber—Part 1: literature review and methodology, Fire Saf. J. 128 (2022), https://doi.org/10.1016/j.firesaf.2022.103523.

[22] G. Heskestad, Modeling of enclosure fires, Symposium (International) Combust. 14 (1973) 1021–1030, https://doi.org/10.1016/S0082-0784(73)80092-X.

[23] D. Gross, A.F. Robertson, Experimental fires in enclosures, Symposium (International) Combust. 10 (1965) 931–942, https://doi.org/10.1016/S0082-0784(65)80236-3.

[24] J.P. Hidalgo, C. Maluk, A. Cowlard, C. Abecassis-Empis, M. Krajcovic, J.L.J. L. Torero, A Thin Skin Calorimeter (TSC) for quantifying irradiation during large-scale fire testing, Int. J. Therm. Sci. 112 (2017) 383–394, https://doi.org/10.1016/j.ijthermalsci.2016.10.013.

[25] I. Pope, J.P. Hidalgo, R.M. Hadden, J.L. Torero, A simplified correction method for thermocouple disturbance errors in solids, Int. J. Therm. Sci. 172 (2022) 107324, https://doi.org/10.1016/j.ijthermalsci.2021.107324.

[26] B.J. Mccaffrey, A robust bidirectional low velocity probe for flame and fire application, 26 125–127, https://doi.org/10.1016/0010-2180(76)90062-6, 1976.

[27] V. Gupta, Open-Plan Compartment Fire Dynamics, The University of Queensland, 2021.

[28] D. Drysdale, An Introduction to Fire Dynamics, third ed., Wiley, 2011 https://doi.org/10.1016/0379-7112(86)90046-9.

[29] A. Nasr, S. Suard, H. El-Rabii, J.P. Garo, L. Gay, L. Rigollet, Heat feedback to the fuel surface of a pool fire in an enclosure, Fire Saf. J. 60 (2013) 56–63, https://doi.org/10.1016/j.firesaf.2012.12.005.

[30] J.G. Quintiere, B.J. McCaffrey, The Burning of Wood and Plastic Cribs in an Enclosure: Volume I, Washtington DC, 1980.

[31] T.Z. Harmathy, Experimental study on the effect of ventilation on the burning of piles of solid fuels, Combust. Flame 31 (1978) 259–264, https://doi.org/10.1016/0010-2180(78)90138-4.

[32] S. McAllister, Burning rate and flow resistance through porous fuel beds: axisymmetric versus line fires, Combust. Sci. Technol. 195 (2023) 3148–3167, https://doi.org/10.1080/00102202.2021.2019233.

[33] J.P. Hidalgo, T. Goode, V. Gupta, A. Cowlard, C. Abecassis-Empis, J. Maclean, A. I. Bartlett, C. Maluk, J.M. Montalvá, A.F. Osorio, J.L. Torero, The Malveira fire test: full-scale demonstration of fire modes in open-plan compartments, Fire Saf. J. 108 (2019), https://doi.org/10.1016/j.firesaf.2019.102827.

[34] J. Luo, K. Ying, J. Bai, Savitzky-Golay smoothing and differentiation filter for even number data, Signal Process. 85 (2005) 1429–1434, https://doi.org/10.1016/j.sigpro.2005.02.002.

[35] V. Gupta, J.P. Hidalgo, A. Cowlard, C. Abecassis-Empis, A.H. Majdalani, C. Maluk, J.L. Torero, Ventilation effects on the thermal characteristics of fire spread modes in open-plan compartment fires, Fire Saf. J. 120 (2021) 1–9, https://doi.org/10.1016/j.firesaf.2020.103072.

[36] S. Welch, A. Jowsey, S. Deeny, R. Morgan, J.L. Torero, BRE large compartment fire tests-characterising post-flashover fires for model validation, Fire Saf. J. 42 (2007) 548–567, https://doi.org/10.1016/j.firesaf.2007.04.002.

[37] J. Prahl, H.W. Emmons, Fire induced flow through an opening, Combust. Flame 25 (1975) 369–385, https://doi.org/10.1016/0010-2180(75)90109-1.

[38] K.D. Steckler, J.G. Quintiere, W.J. Rinkinen, Flow induced by fire in a compartment, Symposium (International) Combust. 19 (1982) 913–920, https://doi.org/10.1016/S0082-0784(82)80267-1.

[39] C. Huggett, Estimation of rate of heat release by means of oxygen consumption measurements, Fire Mater. 4 (1980) 61–65, https://doi.org/10.1002/fam.810040202.

[40] G. Kanellopoulos, A. Bartlett, A. Law, Investigation into global equivalence ratio and external plumes from timber lined compartments. Proceedings of the Ninth International Seminar on Fire and Explosion Hazards (ISFEH9), 2019, pp. 468–477.